AAS 14-446

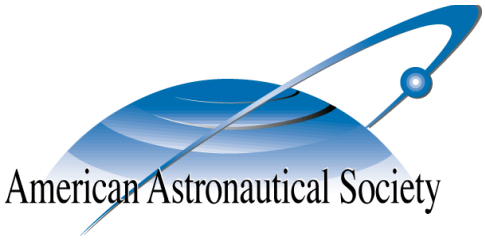

American Institute of
Aeronautics and Astronautics

DISCRETIZED INPUT SHAPING FOR A LARGE THRUST TETHERED DEBRIS OBJECT

Lee Jasper and Hanspeter Schaub

AAS/AIAA Space Flight Mechanics Meeting

Santa Fe, NM **January 26 - 30, 2014**

AAS Publications Office, P.O. Box 28130, San Diego, CA 92198

AAS 14-446

DISCRETIZED INPUT SHAPING FOR A LARGE THRUST TETHERED DEBRIS OBJECT

Lee Jasper* **and Hanspeter Schaub†**

Towing objects in space has become an increasingly common concept for many missions. Asteroid retrieval, satellite servicing, and debris removal concepts often rely on a thrusting vehicle to redirect and steer a passive object. One effective way to tow the object is through a tether. This study employs a discretized tether model attached to six degree-of-freedom end bodies. To reduce the risk of a post-burn collision between the end bodies, thrust input shaping methods using continuous, discrete, and impulsive thrust profiles are considered. On-orbit simulations in a near-Earth orbit show the tethered system achieves oscillations about a gravity gradient alignment, reducing the post-burn collision likelihood. Continuous input shaping thrust profiles perform desirably, avoiding post-burn collision between the end bodies. However, they are not realistic for current day rocket engine capabilities. Impulsive input shaping profiles are considered because thrusters cannot attain continuous thrust-level modifications. Nevertheless, impulsive input shaping techniques attain similar performance by avoiding collisions and inducing gravity gradient motion of the system.

INTRODUCTION

The concept of towing objects in space has been gaining interest because it is useful for a variety of mission concepts. NASA has proposed several missions to asteroids to study them while developing deep-space exploration techniques (NASA FY2014 Complete Budget*). However, NASA also wants to retrieve an asteroid and return it to a near Earth orbit for easier access.[1] There are several ideas for capturing the asteroid; however, the process of imparting Δv to the object has received less attention. Towing also has been proposed for satellite servicing as well as Active space Debris Removal (ADR).[2] The beneficial effects of reducing debris growth by using ADR is being actively investigated.[3,4,5] Another active research avenue for ADR are the many challenging questions about the process of attaching to debris.[2,6,7,8] However, there are fewer studies of what orbit burns to perform to change the debris' orbit while maintaining a low collision risk. This paper addresses the dynamics and open-loop thrusting control of towing large end bodies in space while considering both continuous and discrete/impulsive thrusting profiles.

The tethered-tug concept discussed here focuses on space debris-like objects. However, the basic concept is applicable to small asteroid and satellite towing mission concepts. Figure 1 demonstrates the towing mission concept where a craft, capable of actively thrusting (referred to as the 'tug'), is tethered to the passive object: debris, asteroid, or satellite to be serviced.

*Ph.D. Candidate, Aerospace Engineering Sciences Department, University of Colorado, Boulder, CO USA.
†Professor, Aerospace Engineering Sciences Department, University of Colorado, Boulder, CO USA.
*http://www.nasa.gov/news/budget/index.html

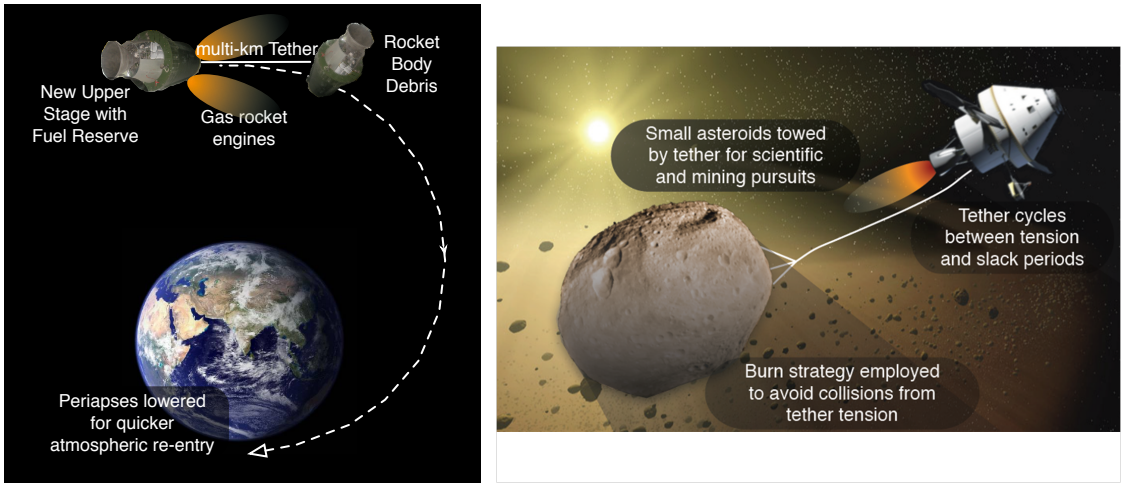

(a) Tethered ADR concept with rocket bodies

(b) Tethered Tug with a small asteroid

Figure 1. Examples of tethered tug concepts

When specifically considering the ADR mission, Figure 1(a), the tug could be a rocket that is assumed to have deployed its payload and completed its primary mission. Its secondary mission goal is to use the remaining fuel reserves to rendezvous with a debris object with similar orbital parameters. After attaching a tether to the debris object the tug thrusts, lowering the periapsis of both objects. The tug will then change the periapsis so that drag forces cause both objects to deorbit within 25 years. Depending upon initial starting altitude and amount of reserve fuel available to the active upper stage, the debris-tug system could be deorbited within half an orbit.[9,10,11]

There have been several proposed ADR methods[2,6,7,8,9,11] that utilize harpoons, mechanical grapples, or nets to grab the debris object. There has been particularly encouraging results from the Astrium Harpoon system[12] demonstrating the capability to penetrate metal while supporting large loads. While the study of the debris capture system is beyond the scope of this research, all of these methods are likely to use tethers to connect the debris to the ADR craft because tethers are a very effective means to change the orbital momentum of on-orbit objects.

One of the primary challenges of the tethered-tug system is collision avoidance between the end bodies. During the thrusting maneuver the tether is strained. When the thrust is no longer present the tether will restore itself to zero strain, pulling the tug and debris together. References 9 and 13 show the strain-collision behavior in more detail. Therefore, it is important to reduce post-thrust strain and relative motion between the bodies to remove collision potential. This is done through input shaping of the open-loop thrust profile. An input shaped control or thrust profile can be designed such that the primary natural frequency(ies) of the flexible body are not excited by the control input.[14,15] Figure 2 shows the thrusting profiles considered in this paper including a step input (Figure 2(a)), continuously notched input (Figure 2(b)), a discrete thrust level based upon the notch which also behaves like a Posicast controller (Figure 2(c)), and an impulsive/bang-bang method (Figure 2(d)).

There have been multiple studies of input shaping on flexible bodies, primarily led by Singhose or Singh.[14,15,16,17,18,19,20] Jasper and Schaub[13] demonstrate the effectiveness of an input shaping strategy using a continuously varying thruster profile on the tethered-tug system while creating a very robust control to variable debris, or asteroid, mass. However, this continuous, smooth thrust

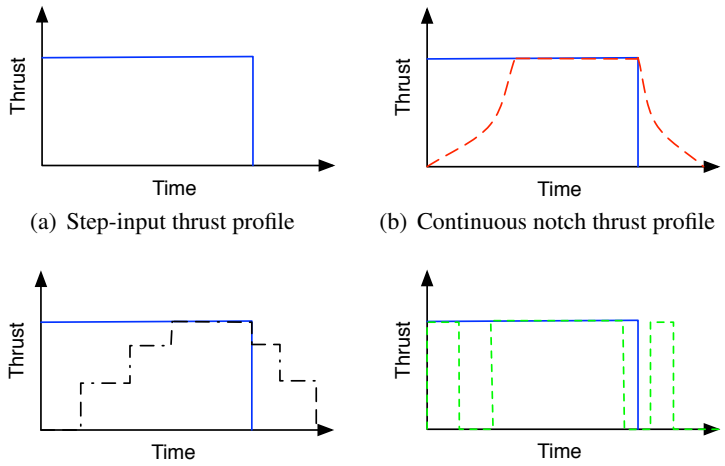

(a) Step-input thrust profile

(b) Continuous notch thrust profile

(c) Discretized notch and Posicast thrust profile

(d) Impulsive thrust profile

Figure 2. Example thrust profiles considered

profile is unachievable by current-day engines. The improved post-burn dynamics such as reduced jerk on the tether attachments and faster settling onto a smooth nadir-aligned oscillation shown with this continuous thrust shaping motivate exploring discretized and bang-bang input shaping thrust profiles. The discretized thruster profile could be implemented with a cluster of thrusters. For example, having 3 thrusters that can be turned on individually would provide 3 discrete levels of thrust. The bang-bang thruster profile with time delays would be suitable for a single on-off thruster implementation. Watanabe et. al[21] and Singhose[14] have also specifically demonstrated input shaping for tethered systems. These studies focus on convolution of multiple impulses to achieve the desired performance. This paper expands upon these studies by analyzing convolution of multiple delay transfer functions, known as a Posicast system, and how such an open-loop deorbiting thrust profile is applicable for space-based towing applications. Bang-bang input shaping is also explored in high-thrust environments with rigid body end masses. Further, the continuous notch profile presented by Reference 13 is discretized so that only a set of discrete thrust-level steps are implemented. The later is considered as a simple reference case to illustrate the benefits of the more rigorous discrete-step and bang-bang input shaping profiles. The effectiveness of the input shaping methods is analyzed in deep-space simulations to understand the difference in performance between each method. On-orbit studies are then explored to consider the low Earth orbit ADR application.

TETHERED-TUG SYSTEM MODEL

The tethered-tug system consists of a thrusting vehicle, the object to tow, and a tether between the two (Figure 1). The tug and the towed object are modeled as rigid bodies that are capable of rotation and translation. The tether is then discretized into multiple lumped point masses connected by visco-elastic forces, as shown in Figure 3.

The tether starts taut at the beginning of thrusting in this study because a slack tether results in an undesirable whipping behavior.[9,13] Further, the thrusting body has active attitude control to ensure the thrust vector points in the desired direction, while thrusting occurs. The attitude control is turned off when the thruster is off.

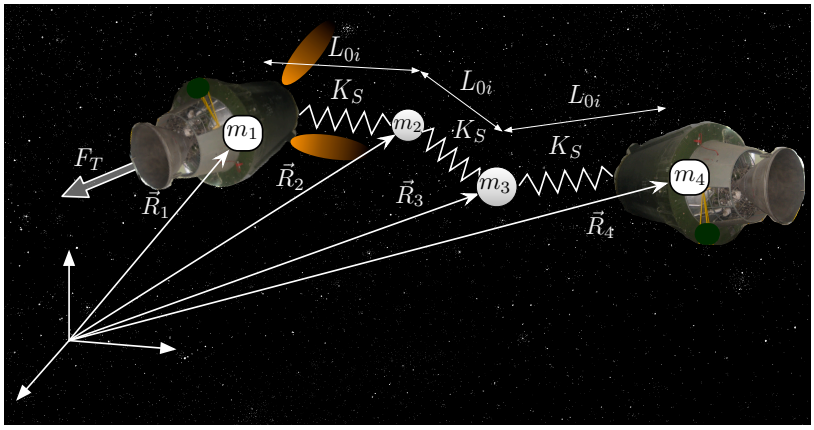

Figure 3. Discretized tether model example with 2 tether masses

Discretized Tether Model

The analysis of tethered systems (also known as Tethered Systems in Space or TSS) is often broken into three models to describe tether motion: continuum, finite element, and discrete mass.[22] Continuum models usually consider partial differential equations and the solutions to these are either extremely difficult to analytically solve or are beyond the scope of this research. Finite element models (FEM) can produce high-accuracy results, however their proper implementation can be difficult and FEM is generally computationally intensive. This research focuses on the gross behavior of a space tether which can be adequately described with discretely lumped masses which approximate the tether flexing and whipping.

Discrete-mass representations of tethers are used frequently. Reference 23 creates a discrete mass model to describe a distributed, tethered infrared telescope. Their system differs from the tethered-tug because it is a rotating, variable tether length system. Further, Reference 23 only considers small point masses on the ends of the tethers. The tethered-tug research considers a very different formation with large rigid body end masses, providing different, challenging dynamics. Williams[22] provides a very similar discrete mass tether to what is used within this thesis research, however Williams' tether is designed as a space elevator anchored to the Earth. The towing system explored here focuses on tether lengths that are much smaller with vastly different end mass behavior. Tethers have been used underwater for years, and there are even similar discrete mass models developed for these underwater tethers.[24,25,26] However buoyancy, surface wave motion, and other environmental inputs create different dynamics. The system developed for this research is capable of modeling higher-order tether modes while capturing large rigid end body motion on both ends of the tether. Further, this research focuses on towing large bodies, something that has not been studied.

The translational equations of motion, caused by the tether, for the system in Figure 3 can be

expressed as

$$\begin{aligned}
\ddot{\boldsymbol{R}}_i &= \tfrac{1}{m_i}\left(K_S(|\boldsymbol{R}_{i+1}-\boldsymbol{R}_i|-L_{0,i})\hat{e}_{i,i+1}\right)\\
\ddot{\boldsymbol{R}}_{i+1} &= \tfrac{1}{m_{i+1}}\left(K_S(|\boldsymbol{R}_{i+2}-\boldsymbol{R}_{i+1}|-L_{0,i+1})\hat{e}_{i+1,i+2}-m_i\ddot{\boldsymbol{R}}_i\right)\\
&\vdots\\
\ddot{\boldsymbol{R}}_N &= \tfrac{1}{m_N}\left(-K_S(|\boldsymbol{R}_N-\boldsymbol{R}_{N-1}|-L_{0,N})\hat{e}_{N-1,N}\right)
\end{aligned} \tag{1}$$

where N is the number of masses and $\hat{e}$ defined as

$$\hat{e}_{i,j} = \frac{\boldsymbol{R}_j - \boldsymbol{R}_i}{|\boldsymbol{R}_j - \boldsymbol{R}_i|} \tag{2}$$

These are only part of the equations of motion used for the numerical simulation used in this paper. Gravity and the thrust control acceleration are also present as well as the rigid body dynamics for the tug and debris.

The natural frequency ω_n of the system can be found by taking the complicated three-dimensional model in Figure 3 and simplifying it to a one-dimensional problem, as in Figure 4.

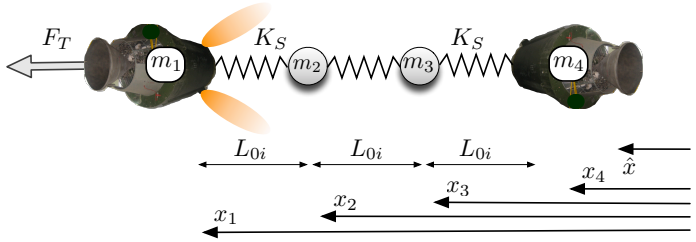

Figure 4. Discretized tether model example with 2 tether masses

The separation between the bodies can now be expressed as

$$\begin{aligned}
L_i &= |\boldsymbol{R}_{i+1}-\boldsymbol{R}_i| - L_0\\
L_i &= x_{i+1} - x_i - L_0\\
\\
\dot{L}_i &= \dot{x}_{i+1} - \dot{x}_i\\
\ddot{L}_i &= \ddot{x}_{i+1} - \ddot{x}_i
\end{aligned} \tag{3}$$

assuming all unstretched tether lengths, L_0, are the same. $\boldsymbol{R}_i$ is the position vector of mass i. Using the linearization in Eq. (3), the discrete mass model in a state space representation is given in Eq. (4). Here n is the number of links between each mass. Therefore, if there are four masses ($N = 4$), there are three tether links and $n = 3$.

$$\dot{\boldsymbol{X}} = [A]\boldsymbol{X} + [B]\boldsymbol{u} \tag{4}$$

The variables in Eq. 4 are given below.

$$\boldsymbol{X}_{2n\times 1} = \begin{bmatrix} L_1 \\ \vdots \\ L_n \\ \dot{L}_1 \\ \vdots \\ \vdots \\ \dot{L}_n \end{bmatrix} \quad [B]_{2n\times 1} = \begin{bmatrix} 0 \\ \vdots \\ 0_n \\ 1 \\ 0_2 \\ \vdots \\ 0_n \end{bmatrix} \quad \boldsymbol{u} = \frac{F_T}{m_1}$$

F_T is the thrust force, applied only to m_1. The matrix $[A]$ can be broken up into four smaller matrices:

$$[A]_{2n\times 2n} = \begin{bmatrix} [0]_{n\times n} & [I]_{n\times n} \\ [A_{2,1}]_{n\times n} & [0]_{n\times n} \end{bmatrix}$$

The acceleration caused by the visco-elastic spring force is given in Eq. 5, is entirely position dependent.

$$[A_{2,1}] = K_S \begin{bmatrix} -\frac{(m_i+m_{i+1})}{m_i m_{i+1}} & \frac{1}{m_{i+1}} & 0_{n-1} & \cdots & 0_n \\ \frac{1}{m_{i+1}} & -\frac{(m_{i+1}+m_{i+2})}{m_{i+1}m_{i+2}} & \frac{1}{m_{i+2}} & \ddots & \vdots \\ 0_{n-1} & \ddots & \ddots & \ddots & 0_{n-1} \\ \vdots & \ddots & \frac{1}{m_{n-1}} & -\frac{(m_{n-1}+m_n)}{m_{n-1}m_n} & \frac{1}{m_n} \\ 0_n & \cdots & 0_{n-1} & \frac{1}{m_n} & -\frac{(m_n+m_{n+1})}{m_n m_{n+1}} \end{bmatrix} \tag{5}$$

m_i is each body's mass and the spring constant K_S is expressed in Eq. (6)

$$K_S = \frac{EA}{L_0} \tag{6}$$

with units of $\frac{N}{m}$. Here L_0 is the initial, unstretched (equidistant) length of the tether between each mass, E is the Young's modulus of elasticity for the tether, and A is the cross sectional area. Because Eq. (4) models a tether as a spring, it is only accurate while the tether is in tension. When the separation distance is less than L_0, all spring forces go to zero. This is also only correct while in tension. There is no damping present while the separation between two masses is less than L_0.

Tether Modes

Input shaping relies upon knowledge of a system's fundamental modes. The model of the system is based upon a linear spring-mass system (when in tension) allowing for easy computation of the modes through Eigenvalue analysis. However, as more nodes are added to the tether, the characteristic equation for the Eigenvalue analysis becomes difficult to analytically solve.[27,28] Adding more than two or three nodes to the tether will make the system not analytically solvable for the higher order modes. Because the first mode of the system contains the most energy, the inability to find the higher modes is not overly important and does not reduce the performance of input shaping.[13]

As an example, the Eigen-frequencies ω_n of a three body (single tether mass) system are:

$$\omega_n = \begin{pmatrix} 0 \\ 0 \\ \pm\sqrt{K_S Z_1 + K_S Z_2} \\ \pm\sqrt{K_S Z_3 + K_S Z_4} \end{pmatrix} \tag{7}$$

where

$$\begin{aligned} Z_1 &= \frac{(m_2 m_3 + m_1(m_2+2m_3))}{2m_1 m_2 m_3} \\ Z_2 &= \frac{\sqrt{m_1^2 m_2^2 - 2m_1 m_2^2 m_3 + (4m_1^2+m_2^2)m_3^2}}{2m_1 m_2 m_3} \\ Z_3 &= \frac{(-2m_1 m_3 - m_2(m_1+m_3)}{2m_1 m_2 m_3} \\ Z_4 &= \frac{\sqrt{-2m_1 m_2^2 m_3 + m_2^2 m_3^2 + m_1^2(m_2^2+4m_3^2)}}{2m_1 m_2 m_3} \end{aligned}$$

The repeated 0 roots relate to the DC offset present in the formulation of Eq. (4). Because Eq. (4) is formulated from the positions of the bodies, the equations naturally assume that zero tether force corresponds to separation distances between the masses that add up to the full tether length (i.e. L_0). Therefore the bodies have a constant, DC offset in their positions. The complex pair(s) in Eq. (8) represent the purely oscillatory motion, as expected from a spring-mass system. Eq. (8) has two sets of complex pairs due to the fact that a three body (single tether node) system has two modes: one from the full tether length and one from the addition of the tether mass.

TUG THRUSTER INPUTER SHAPING METHODS

Continuous Input Shaping Overview

Reference 13 found that the first fundamental mode of the tethered tug system causes the most motion between the bodies. By creating a doubly notched thrust profile, where the notched frequencies span a range around the fundamental mode, a robust control design that can withstand errors in knowledge of the mass of the towed object. This is very advantageous because the mass of a debris object or an asteroid is likely to only be an approximate value. The double notch filter is used throughout this paper for the 'continuous' and 'discrete' notch controls.

A double notch allows for knowledge errors in the mass of the towed object, which are likely when towing an asteroid or debris. A double notch is effectively created by notching two frequencies at once or by multiplying two notch filters together, in the frequency domain, that have different cut-off frequencies. (This places two zeros around the primary pole of the system.)

$$g(s) = \frac{(s^2 + \omega_{c1}^2)(s^2 + \omega_{c2}^2)}{(s^2 + \mathrm{BW}_1 s + \omega_{c1}^2)(s^2 + \mathrm{BW}_2 s + \omega_{c2}^2)} \tag{8}$$

where s is the frequency, ω_{c1} is the first cut-off or notch frequency, ω_{c2} is the second cut-off or notch frequency, and $BW1$ and $BW2$ are the bandwidths for each notch. (Performing an Eigen value analysis on the dynamics matrix $[A]$ in Eq. (4) yields the natural frequency that the double notch should be centered around.) Eq. (8) can be converted into the discrete domain and the time domain in many ways. This process is not discussed here, but a trapezoidal differencing method is used.[29]

The frequency domain response of the double notch can be seen in Figure 5 (see Table 1 for simulation parameters). The center frequency range was determined by an Eigen value sensitivity analysis to a change in debris mass. Reference 13 shows that an expected tow mass of 1500 kg can vary by as much as ± 500 kg and still see minimal relative motion between the two end bodies, when using a double notch.

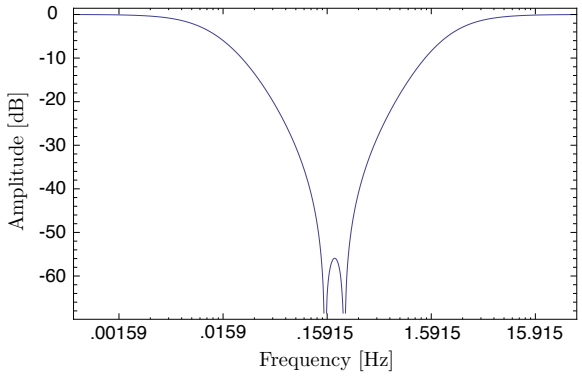

Figure 5. Double notch centered about first fundamental mode of system

With this method, the thruster throttle is assumed to be capable of achieving all thrust magnitudes that are commanded. This is unrealistic for present day high-thrust engines which are only able to operate in on-off control modes. Because of this fact, three other thrusting methods are presented. The first method simply takes the desired continuous double notch profile (Figure 2(b)) and discretizes it (Figure 2(c)). The performance of this method becomes a benchmark to compare the following two more rigorous input shaping methods. The second method uses a Posicast control that also behaves similarly to Figure 2(c). Here the tug is assumed to have a cluster of several thrusters that can be engaged individually. Finally, a bang-off-bang profile (Figure 2(d)) is used. This scenario assumes a single thruster is present, but it can be turned on and off again repeatedly. While the discretized notch profile attempts to behave like the notch, the Posicast and bang-off-bang profiles are designed to remove the undesired frequencies and therefore are more rigorous formulations.

Discretized Thrust Input Shaping

For the discretized input shaping control, it is assumed the thruster is only capable of a set number of thrust levels. For example, with a cluster of 4 equal thrusters, the open-loop towing control is only capable of stepping the net thrust in 25% increments of the maximum thrust available. This is implemented by having each thruster individually turn on or off at the desired times. The continuous model is used as the desired thrust profile but the actual profile is set to specific magnitudes given a thrust step size. The basic algorithm is given in Eq. 9.

$$\begin{aligned} \text{step size} &= T_{\text{step}} \\ \text{desired thrust} &= T_{\text{desired}} \\ \tau_{\text{ratio}} &= \text{Mid-Point Rounding}\left(\tfrac{T_{\text{desired}}}{T_{\text{step}}}\right) \\ T_{\text{applied}} &= \tau_{ratio} * T_{\text{step}} \end{aligned} \tag{9}$$

The algorithm uses a simple rounding method. The rounding scheme in Eq. 9 uses a mid-point method so that if the desired thrust is greater than 50% of T_{step}, then the applied thrust will jump

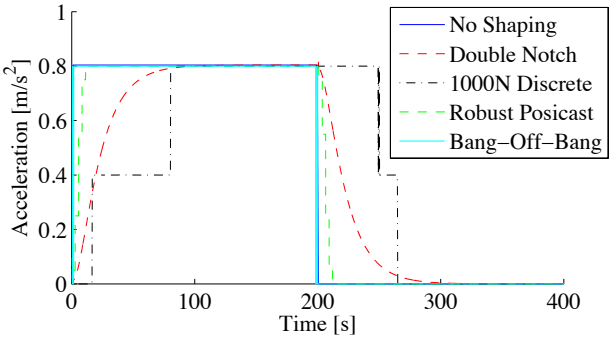

Figure 6. Applied thrust profiles with different input shaping techniques

to the next step size, otherwise the applied thrust remains at the previous level. This causes the desired thrust to be *above* each step size to achieve a new T_{applied} level. The difference between the continuous and discrete applied thrust is demonstrated by Figure 6.

Posicast Input Shaping

As shown by Singh,[15] a time delay system can be used as an open loop control on a system.

$$A_0 + \sum_{i=1}^{N} A_i e^{-sT_i} = 0 \tag{10}$$

Singh demonstrates a number of Posicast methods to properly actuate a system, as well as make the control more robust to modeling errors. Singh also generally considers moving a system from one position to another. However, this paper expands upon these works by formulating a robust Posicast, open-loop input shaper, that achieves a desired velocity without exciting natural frequencies. Because the first mode of the tethered system has been shown to be the most important,[13] a Posicast controller is developed only for the first mode.

The Posicast input shaping profile operates on the assumption that a step input control/thrust profile is given to the controller. The controller then takes the step and manipulates it so that it does not excite undesirable modes. The thrust profile created by the Posicast control is shown in Figure 6 but in the time scale shown, it is harder to differentiate between the impulsive profiles and the step input. It should be emphasized that the Posicast profile *does* behave similarly to the illustration in Figure 2(c).

Assuming there are only two end bodies with a spring force between them, the equations of motion are simplified to:

$$\begin{aligned} \ddot{x}_1 &= \tfrac{1}{m_1}\left(K(x_2 - x_1 - L_0) - F_T\right) \\ \ddot{x}_2 &= \tfrac{1}{m_2}\left(-K(x_2 - x_1 - L_0)\right) \end{aligned} \tag{11}$$

The separation distance between the two end bodies is defined as $L = x_2 - x_1 - L_0$, where L_0 is the unstretched length, a constant. The resulting tether flexing dynamics is written as

$$\begin{aligned} \ddot{L} &= \ddot{x}_2 - \ddot{x}_1 \\ \ddot{L} &= -K\tfrac{m_1+m_2}{m_1 m_2} L + \tfrac{F_T}{m_1} \end{aligned} \tag{12}$$

where $\sqrt{K\frac{m_1+m_2}{m_1m_2}}$ is the natural frequency of a two body spring-mass system. Taking the Laplace Transform of the system in Eq. (12) gives the transfer function

$$H(s) = \frac{L}{u(s)} = \frac{1}{s^2 + K\frac{m_1+m_2}{m_1m_2}} \tag{13}$$

Eq. (13) shows that the poles of the system occur at $s = \pm\sqrt{-K\frac{m_1+m_2}{m_1m_2}} = \pm j\omega_n$, where $j = \sqrt{-1}$. The most basic Posicast controller uses only one time delay and is solved as an example. A single delay takes the form

$$A_0 + A_1 e^{-sT} = 0 \tag{14}$$

Plugging in s to Eq. (10) the exponential term can be written as

$$e^{j\omega_n T} = \cos(\omega_n T) + j\sin(\omega_n T) \tag{15}$$

To solve the system, Eq. (15) is separated into real and imaginary components.

$$\begin{array}{cc} \text{Real} & A_0 + A_1\cos(\omega_n T) = 0 \\ \text{Imaginary} & A_1\sin(\omega_n T) = 0 \end{array} \tag{16}$$

This quickly results in the solutions for A_0 and T if A_1 is defined to equal 1, the maximum normalized input.

$$\begin{array}{rc} T = & (2n-1)\frac{\pi}{\omega_n} \\ A_0 = & -\cos(\omega_n T) = -\cos\left((2n-1)\pi\right) \end{array} \tag{17}$$

However, the time delay control from Eq. (14) is very sensitive to modeling errors therefore several delays are given to make the system more robust. To make the system solvable, Singh[15] specifies that each time delay is only a multiple of the single delay T, from Eq. (17). The controller designed for the tethered tug system is shown in Eq. (18).

$$A_0 + A_1 e^{-sT} + A_2 e^{-2sT} + A_3 e^{-3sT} + A_4 e^{-4sT} = 0 \tag{18}$$

To solve this system for the impulse amplitudes, A_i, several equations are required. Note that implementing the system in Eq. (18) would require 5 thrusters, one for each amplitude A_i. The real and imaginary parts are found again, as in Eq. (16). However three more constraints are defined:

$$\begin{array}{rc} \frac{d}{d\omega_n}(\text{Real}) = & 0 \\ \frac{d}{d\omega_n}(\text{Imaginary}) = & 0 \\ A_0 + A_1 + A_2 + A_3 + A_4 = & 1 \end{array} \tag{19}$$

The derivatives of the real and imaginary components of Eq. (18) add robustness by reducing the size of the residual vibration in the system after an input has been added. The constraint that all of the amplitudes sum to one is used so that the input is not scaled but equal to its full value after all delays have occurred. Solving this system of equations, the amplitudes are found to be

$$\begin{array}{rc} A_0 = & \frac{1}{16}\csc\left(\frac{T\omega_n}{2}\right)^4 \\ A_1 = & -\frac{1}{4}\cos(T\omega_n)\csc\left(\frac{T\omega_n}{2}\right)^4 \\ A_2 = & \frac{1}{8}(2+\cos(2T\omega_n))\csc\left(\frac{T\omega_n}{2}\right)^4 \\ A_3 = & -\frac{1}{4}\cos(T\omega_n)\csc\left(\frac{T\omega_n}{2}\right)^4 \\ A_4 = & \frac{1}{16}\csc\left(\frac{T\omega_n}{2}\right)^4 \end{array} \tag{20}$$

To turn this development into a velocity control instead of a position control, the amplitudes from Eq. (20) are used at the beginning and end of the step input thrust profile to achieve a ramping on and off as shown in Figure 2(c). The duration of the burn is nearly the same as the step input but is extended by $8T$ to account for the ramp on/off behavior.

Bang-off-bang Input Shaping

The bang-off-bang controller creates a profile that can be implemented by a single thruster that can repeatably be turned on and off. This method also assumes that a step input is given to the controller that is then modified to not excite system modes. Singh[15] demonstrates several ways to create a bang-off-bang controller; however, the basic principle is to find a linear system's state transition matrix and control matrix. Combining these matrices with several constraints, like those in Eq. (19), yields a system that can be solved as a linear programming problem. Full details are given by Singh, however, an abbreviated derivation is given for clarity. Further, the thrust profile is shown in Figure 6 but is better illustrated by Figure 2(d).

Given initial and final conditions, $\boldsymbol{x}_0$ and $\boldsymbol{x}_f$ and a system of the form in Eq. (4), the problem can be set up as follows. We wish to minimize the maneuver time, so

$$\text{Minimize } f^T t \tag{21}$$

where t is the maneuver time vector and f is a vector that defines the given time we wish to minimize. In this case, since it is desired to minimize the total time, f is a vector of zeros except the last value, which is a 1 corresponding to the last time. Singh then discretizes the continuous system of Eq. (4), obtaining

$$\boldsymbol{x}_{k+1} = [A_D]\boldsymbol{x}_k + [B_D]\boldsymbol{u}_k \tag{22}$$

where $[A_D]$ is the discrete dynamics matrix and $[B_D]$ is the discrete control matrix. Writing the system in terms of the initial condition

$$\boldsymbol{x}_{k+1} = [A_D]\boldsymbol{x}_0 + \sum_{i=1}^{k} [A_D]^{k-i}[B_D]\boldsymbol{u}_i \tag{23}$$

The summation of inputs can be rewritten and solved for as a matrix giving

$$\begin{bmatrix} [A_D]^{N-1}[B_D] & [A_D]^{N-2}[B_D] & \cdots & [A_D][B_D] & [B_D] \end{bmatrix} \begin{bmatrix} u_1 \\ u_2 \\ \vdots \\ u_N \end{bmatrix} = \boldsymbol{x}_f - [A_D]^N \boldsymbol{x}_0 \tag{24}$$

The system given in Eq. (24) allows the user to specify the initial and final conditions ($\boldsymbol{x}_0$, $\boldsymbol{x}_f$) and it is solvable using linear programming techniques, in the form of $M\boldsymbol{u} = b$. However to be useful as a bang-off-bang system, several additional constraints are required. One is that the inputs end in either zero or one. This is enforced by adding a row to $[M]$ that is all zeros except for the last column, which is a one. The $[b]$ matrix also has an additional value added that is either a zero or one. This allows for the final control value u_N to be specified as whatever value is designated in $[b]$. The second constraint is on the input sizes. To create a bang-off-bang control, the inputs $\boldsymbol{u}$ are required to be bounded between zero and one. (To create a bang-bang control, the inputs can be

bounded between negative and positive one.) The value of one is used so that the user defined input is used in its entirety and not scaled.

To create a velocity control bang-off-bang profile, the linear programming problem is solved twice. To begin thrusting while avoiding exciting system modes

- $\boldsymbol{x}_0 = 0$
- $\boldsymbol{x}_f = L_1$
- The final input u_N is specified to be 1

The value L_1 is defined simply from the approximate separation distances seen from the other control methods, like the continuous notch. The tether usually ends up stretching less than a meter, for a 1000 m tether. The selection of this value does not drastically affect the performance of the system, unless it is larger than the stretch distance possible given the thrust magnitude and the tether material properties. The final control input is kept at one for the burn duration to achieve the desired Δv. The linear programming problem is then solved again to end thrusting using

- $\boldsymbol{x}_0 = L_1$
- $\boldsymbol{x}_f = 0$
- The final input u_N is specified to be 0

NUMERICAL SIMULATION RESULTS

To demonstrate the effectiveness of each thrusting method (continuous, discretized, and impulsive), numerical simulations are performed. The basic system parameters are given in Table 1 and are modeled after a Soyuz upper stage for the tug vehicle, and a Cosmos rocket body for the debris object.

Table 1. Vehicle, Tether and Simulation Parameters

Tug Mass	2500 kg
Tug Inertia	diag[10208, 10208, 2813] kg m^2
Debris Mass	1500 kg
Debris Inertia	diag[1285, 6829, 6812] kg m^2
Tether Length	1000 m equal space between masses
Tether Material	Kevlar
E	1470 GPa
Tether Diameter	3.2 mm
Tether Mass	11.822 kg†
Thrust	2009 N
Δv	100 m/s
Starting Altitude	800 km (circular)

If Eq. 8 is analyzed given the values in Table 1, the natural frequencies of the system are obtained. It is interesting to note that the fundamental frequency is the same between the two-body, three-body, or four-body cases. This turns out to be (for two bodies: $m_1 = 2500$ kg, $m_2 = 1500$ kg; for three bodies: $m_1 = 2500$ kg, $m_2 = 11.82$ kg, and $m_3 = 1500$ kg, for four bodies: $m_1 = 2500$ kg, $m_{2a} + m_{2b} = 5.91 + 5.91 = 11.82$ kg, and $m_3 = 1500$ kg) $\omega_{n1} = 0.19$ Hz. The three node case also has its second mode at $\omega_{n2} = 3.43$ Hz. The first mode is of greatest concern and is the frequency that all input-shaping methods attempt to reduce.

Note that the simulations shown utilize the following:

- The trapezoidal difference method is used to go from the frequency domain to discrete time, for the notch filter input-shapers
- The attitude on the tug (m_1) is maintained while thrusting occurs
- The discretized notch filter uses a mid-point round up discretization (Eq. (9))
- The Δv applied is equal to 100 m/s. Based upon input-shaping method, this can vary the thrusting duration

The time T that results from Eq. (17), and is used to implement the profiles of Eq. (18) and Eq. (24), is about 2.83 s. This means that the Posicast amplitudes change, and the bang-bang profile switches using T as the baseline actuation time. For a five step Posicast system, the ramp on or off takes just over 14 s.

Deep Space Results

Deep space simulations (in the absence of a gravity field) are conducted because they are informative for showing the effectiveness of a given thrusting method. Deep space is also relevant for the asteroid towing concept (Figure 1(b)). When a step input thrust profile is used, as in Figure 2(a), it excites all modes present in the flexible tether system causing relative motion between the two bodies. In deep space, this generally results in a collision. However, input shaping the thrust profile can remove these excitable frequencies from the thrust profile, reducing the relative motion. This is demonstrated in Figure 7. Note that the tether tension profile follows the thrust profile. Further, there is almost no relative motion between the two end bodies, as shown by the separation distance remaining near 1000 m. Figure 7 also considers the double notch with a mass knowledge error of 500 kg (the debris is expected to be 2000 kg but it is really 1500 kg), again showing the effectiveness of this method.

Figure 8 shows four non-continuous thrust system responses. (Figure 6 gives the profiles used.) In Figure 8(a) and Figure 8(b) the continuous notch profile used to generate Figure 7 has been discretized into 100 N and 1000 N steps. The 100 N step size was chosen to study a relatively small discretization that could follow the desired continuous profile somewhat effectively. The 1000 N step size was chosen because it is much more likely that a realistic thruster is capable of a small range of different thrusts. A $\sim$2000 N thrust could be attained by coupling two, 1000 N thrusters and turning them on at desirable times.

Altering the continuous thrust profiles to discrete steps is moderately effective in reducing post-burn relative velocity even when introducing these discrete thrusting steps. The 100 N discretization sees greater than 900 m of separation between the two end bodies, showing that there was only a

[†] http://www.matweb.com/index.aspx

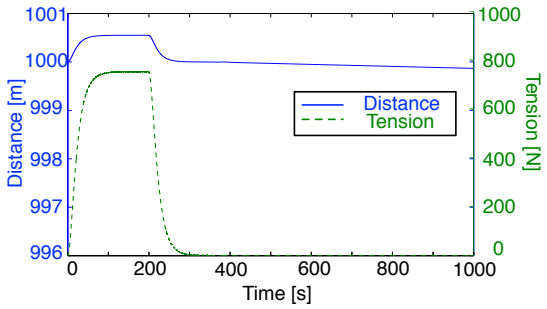

Figure 7. Relative motion and tether tension response between tug and debris using a *continuous* double notch spanning $.14 \leq \omega_c \leq .22$Hz. Expected debris mass of 2000 kg ($\omega_n = .17$ Hz), actual mass is 1500 kg ($\omega_n = .19$ Hz). 2009 N thrust, with 2 discrete tether masses

small amount of tension remaining in the tether at the end of the thrusting duration. However, the much cruder 1000 N discretization of the continuous thrust profile experiences much more relative motion, and a collision between the tug and one of the tether masses at about 1000 s. This shows the 1000 N discretization appears to be too crude of a discretization, even though it is more practical for current-day engine capabilities.

When considering the impulsive input shaping methods in Figure 8(c) and Figure 8(d), it can be seen that these thrust profiles (Figure 6) produce very desirable behavior. The Posicast controller only sees about 7 m of drift over the time span considered, while the bang-off-bang profile sees about 100 m of drift. These results are exciting because they demonstrate that input shaping controllers can be designed with profiles that are more reasonable for current-day engine capabilities.

Figure 9 shows the frequency domain response of the tug mass, given the different thrust profiles. Figure 9(a) shows a step input exciting the modes of the tethered-tug system. The primary mode occurs at 0.19 Hz and has a fairly large magnitude. The double notch in Figure 9(b) reduces this first mode by about two orders of magnitude in power, thus creating the tiny relative motion in Figure 7. The magnitude of the first mode in the 100 N discretized frequency response (Figure 9(c)) is only slightly attenuated from the step input. However, this is enough to produce small relative motion, as shown by Figure 8(a). The 1000 N discretization response (Figure 9(d)) has very little difference from the step input, and therefore experiences a post-burn collision quite quickly. Figure 9(e) shows the Posicast frequency response, which also shows a very attenuated fundamental mode (0.19 Hz), comparable to the continuous double notch in Figure 9(b). This again demonstrates that impulsive input shaping is a viable method to controlling the tethered-tug system. While some other frequencies do appear amplified, they are not around the fundamental mode of the system, and therefore do not adversely affect the system as modeled. Figure 9(f) shows the bang-off-bang frequency response which does not see nearly as much attenuation as the Posicast or double notch profile, but it does attenuate the fundamental mode enough to see reduced relative motion between the two bodies, as shown in Figure 8(d).

On-Orbit Results

Deep space simulations motivate the use of a given thrust profile for on-orbit analyses. However, the orbital dynamics create interesting behavior that is not predicted by deep space analysis, including the tendency toward a gravity gradient, or nadir alignment, of the tethered system.[13] Even

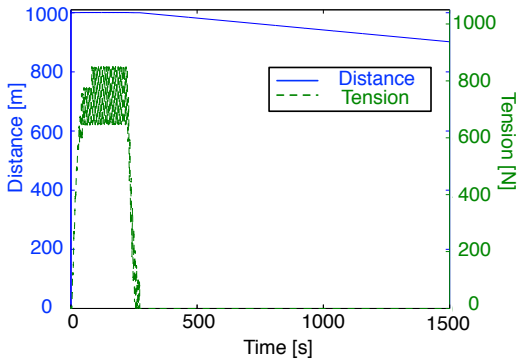

(a) 100 N step *discrete* double notch spanning $.14 \leq \omega_c \leq .22$Hz

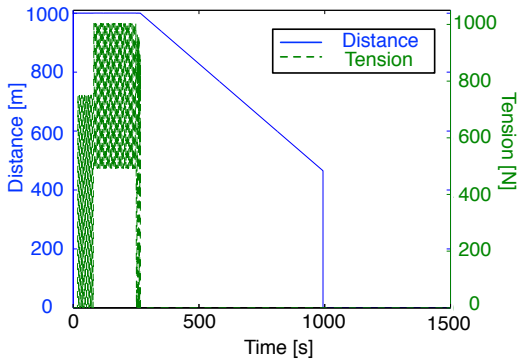

(b) 1000 N step *discrete* double notch spanning $.14 \leq \omega_c \leq .22$Hz, collision at about 1000 s

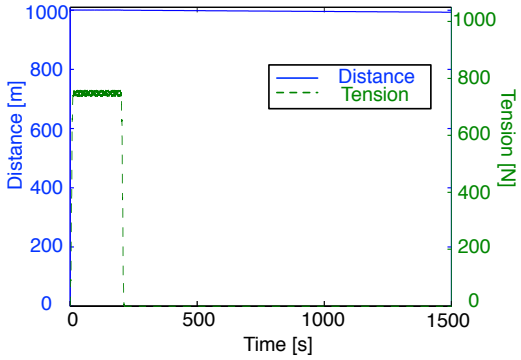

(c) Robust Posicast thrust shaping, Eq. (18)

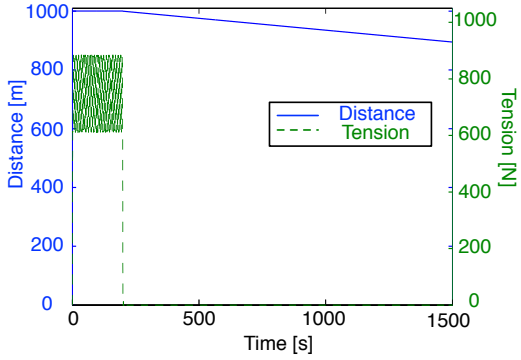

(d) Bang-off-bang thrust shaping, Eq. (24)

Figure 8. Relative motion and tether tension response between tug and debris. Expected debris mass of 2000 kg ($\omega_n = .17$ Hz), actual mass is 1500 kg ($\omega_n = .19$ Hz, green line(s) oscillation frequency). 2009 N thrust, with 2 discrete tether masses

though the 100 N discretized thrust profile had better performance in a deep space environment, it is not realistic performance for a thruster. Therefore, the 1000 N discretization is used in the on-orbit analysis. The 1000 N discretized, Robust Posicast, and bang-off-bang thrust profiles are used, unaltered from their deep-space implementation.

Figure 10 shows the relative separation distance and tension present in the tethered-tug system for a continuous and discrete notch, as well as the two impulsive shaped thrust profile. Reference 13 shows that the continuous notch tends towards a nadir alignment of the system, which is a stable configuration that does not allow the two craft to collide. However, as shown by Figure 10(a) the two end masses do get close before they stabilize into a nadir alignment. What is very exciting about the discretized thruster, Figure 10(b), is that the 1000 N discretized thrust that did not work well in deep space, performs fairly well in orbit. This is likely due to larger differences in relative motion post-maneuver that cause the two craft to stay further separated. Figure 10(c) and Figure 10(d) show the Robust Posicast and bang-off-bang solutions. These again, demonstrate admirable performance as they both achieve gravity gradient motion without having the end bodies approaching each other, as occurs with Figure 10(a). Further, the impulsive methods are more benign experiencing lower tension (1400 N versus more than 2000 N) and faster settling to gravity gradient oscillations with

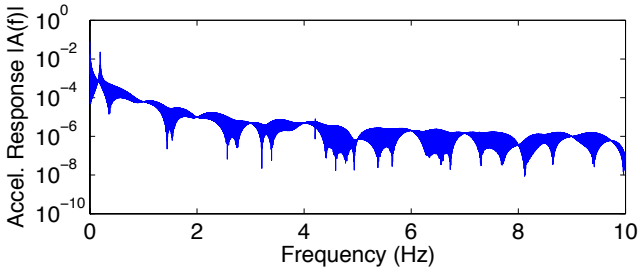

(a) Step-input thrust profile

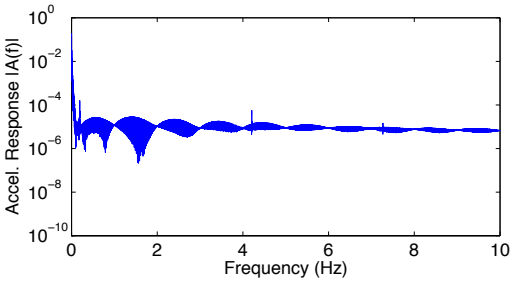

(b) Double notch spanning $.14 \leq \omega_c \leq .22$Hz

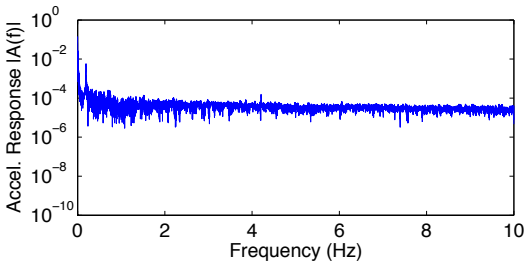

(c) 100 N discretized double notch spanning $.14 \leq \omega_c \leq .22$Hz

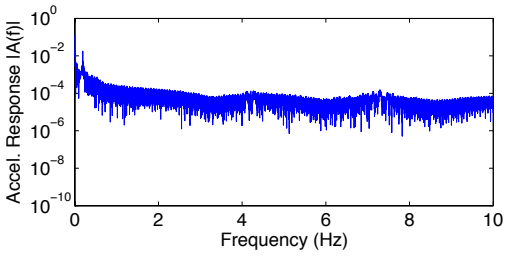

(d) 1000 N discretized double notch spanning $.14 \leq \omega_c \leq .22$Hz

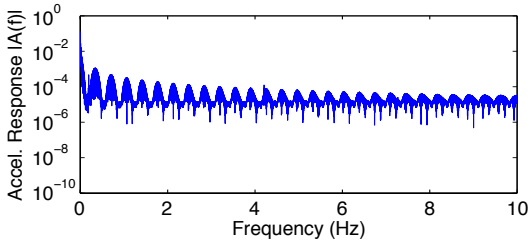

(e) Robust Posicast thrust shaping

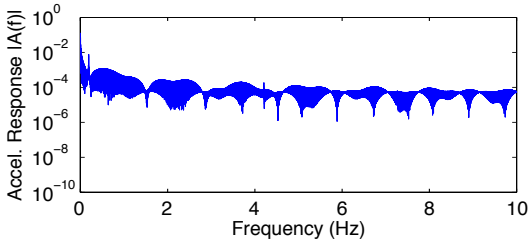

(f) Bang-off-bang thrust shaping

Figure 9. Tug vehicle frequency response to 2009 N thrust, with 2 discrete tether masses, in deep space

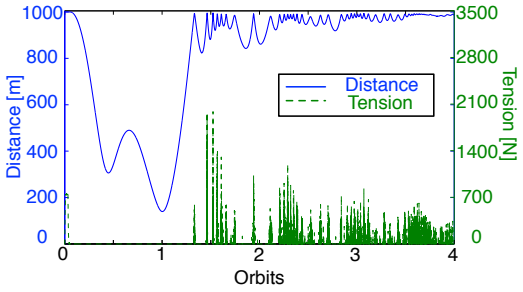

(a) Double notch spanning $.14 \leq \omega_c \leq .22$Hz

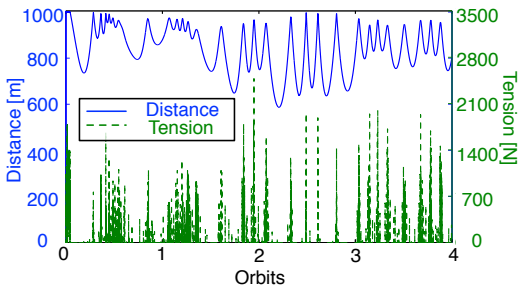

(b) 1000 N discretized double notch spanning $.14 \leq \omega_c \leq .22$Hz

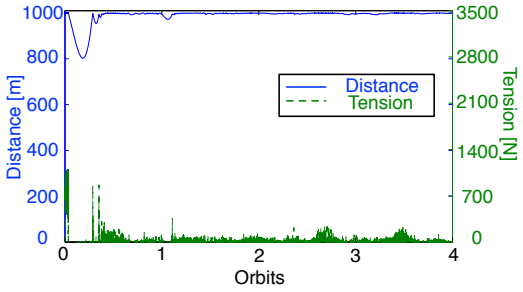

(c) Robust Posicast thrust shaping

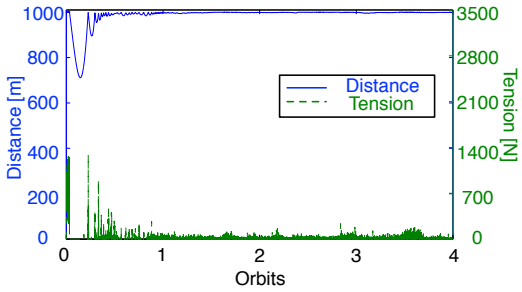

(d) Bang-off-bang thrust shaping

Figure 10. Relative motion and tether tension response between tug and debris for four orbits. Tether $\omega_n = .19$ Hz. 2009 N thrust, with 2 discrete tether masses

end body separations near the full length of the tether.

Figure 11 shows the angle between the end masses and their alignment to nadir. Using that angle as a metric for how well each thrusting method achieves the nadir alignment, it is clear that the 1000 N discretized notch gets close to nadir alignment. The discretized thrust does have more variability in separation distance (Figure 10(a)) between the two end bodies however they will not collide in a nadir alignment. The step input (no shaping) does not settle into a gravity gradient motion and has much more dynamic response, compared to Figure 10.[13] The Robust Posicast and bang-off-bang profiles settle into a gravity gradient oscillation more quickly than either of the notch profiles. Their oscillations are larger, however, the oscillation size is not generally important, as long as the system maintains separation between the bodies. It should be emphasized that no damping is modeled so that the natural tether and end-body dynamics are observed.

CONCLUSION

Towing objects in space through the use of tethers is feasible. Tethered towing can be used for on-orbit servicing and orbit raising, active debris removal, and potentially asteroid retrieval. Avoiding excessive motion and collisions between the two large end masses is critical. A step input thrust creates non-ideal motion and results in collisions, in a deep space environment. Input shaping can effectively reduce the flexing motion of a flexible body as shown by a notch filter that reduces all relative motion and helps the system settle into a nadir alignment when on-orbit. Unfortunately, the continuous thrusting profile required by the notch filter is not realistic with current rocket engine

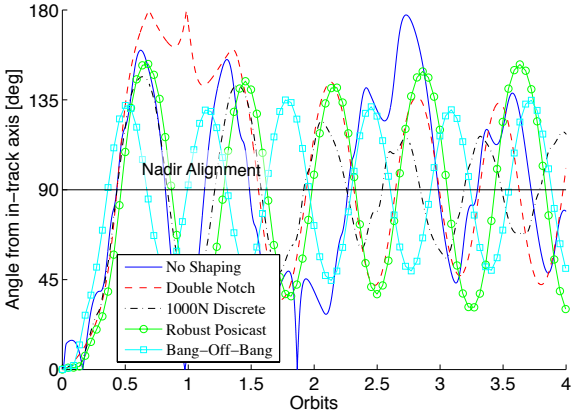

Figure 11. Angle from along-track vector. 90^o is the radial vector

technology. Therefore a discretized version of the notch filter is implemented. In deep space, the discretized thrust achieves variable results depending upon the resolution of the discretization, often encountering end body collision concerns. On-orbit, the discretization helps the system maintain separation distance between the end bodies but it does not achieve an ideal nadir alignment.

The utilization of impulsive input shaping techniques successfully attenuate the first natural frequency of the tethered-tug system providing reduced relative motion and tether tension while being more realistic for current-day rocket technology capabilities. The impulsive techniques are also useful in both deep-space and on-orbit applications, without alteration. This makes these techniques appear incredibly reasonable to use for this system. Further, this paper has shown that a multitude of thrust profiles can be successfully implemented to control this system while avoiding collisions.

ACKNOWLEDGMENTS

The authors would like to acknowledge Valery Trushkyakov, Professor in the Department of Aviation and Rocket Building, Omsk State Technical University for his contributions to the tethered rocket body ADR method.

REFERENCES

[1] K. I. f. Space Studies, *Asteroid Retrieval Feasibility Study*. Smithsonian Astrophysical Observatory, Pasadena, California, 2012.

[2] C. Bonnal and C. R. Koppel, "Getting rid of large debris: a safe low cost alternative," *2nd European Workshop on Active Debris Removal*, Quentin, Paris, France, June 18 – June 19 2012. Paper No. 3.2.

[3] J.-C. Liou and N. L. Johnson, "Risks in space for orbiting debris," *Science*, Vol. 311, 2006, pp. 340 – 341.

[4] J.-C. Liou, N. Johnson, and N. Hill, "Controlling the growth of future LEO debris populations with active debris removal," *Acta Astronautica*, Vol. 66, No. 5-6, 2010, pp. 648 – 653.

[5] J.-C. Liou, "An active debris removal parametric study for LEO environment remediation," *Advances in Space Research*, Vol. 47, No. 11, 2011, pp. 1865 – 1876.

[6] D. Alary, "Astrium's views on OOS & ADR," *European On-Orbit Satellite Servicing and Active Debris Removal Conference*, Brussels, Belgium, October 30 2012.

[7] J. Reed, J. Busquets, and C. White, "Grappling System for Capturing Heavy Space Debris," *2nd European Workshop on Active Debris Removal*, Quentin, Paris, France, June 18 – June 19 2012. Paper No. 4.2.

[8] I. Retat, B. Bischof, J. Starke, W. Froth, and K. Bennell, "Net Capture System," *2nd European Workshop on Active Debris Removal*, Quentin, Paris, France, June 18 – June 19 2012. Paper No. 4.3.

[9] L. Jasper, H. Schaub, C. Seubert, T. Valery, and E. Yutkin, "Tethered Tug for Large Low Earth Orbit Debris Removal," *AAS/AIAA Astrodynamics Specialists Conference*, Charleston, SC, Jan 31 – Feb 2 2012. Paper No. AAS 12-252.

[10] Y. Makarov, A. Ronse, and V. Trushlyakov, "The use of adapted upper stages for the removal of satellite and rocket body debris from unstable orbital regions," *62nd International Astronautical Congress*, Cape Town, South Africa, October 3 – 7 2011. IAC-11,A6,5,10,x10020.

[11] V. Trushlyakov, J. Makarov, G. Raykunov, J. Shatrov, and D. Baranovo, "The development of autonomous onboard systems for the controlled deorbiting of stages separating parts of space launch vehicle," *2nd European Workshop on Active Debris Removal*, Quentin, Paris, France, June 18 – June 19 2012. Paper No. 2.5.

[12] J. Reed and S. Barraclough, "Development of Harpoon System for Capturing Space Debris," *Sixth European Conference on Space Debris*, Darmstadt, Germany, April 22 – 25 2013.

[13] L. Jasper and H. Schaub, "Input Shaped Large Thrust Maneuver with a Tethered Debris Object," Vol. 96, March-April 2014, pp. 128–137.

[14] W. Singhose, "Command Shaping for Flexible Systems: A Review of the First 50 Years," *International Journal of Precision Engineering and Manufacturing*, Vol. 10, No. 4, 2009, pp. 153–168.

[15] T. Singh, *Optimal Reference Shaping for Dynamical Systems, Theory and Applications*. Boca Raton, Florida: CRC Press, 2010.

[16] T. Singh, P. Singla, and U. Konda, "Polynomial Chaos Based Design of Robust Input Shapers," *Journal of Dynamic Systems, Measurement, and Control*, Vol. 132, 2010, pp. 051010–1 – 13.

[17] R. Kumar and T. Singh, "Design of Input Shapers using Modal Cost for Multi-Mode Systems," *Automatica*, Vol. 46, No. 3, 2010, pp. 598–604.

[18] W. Singhose, W. Seering, and N. Singer, "Residual Vibration Reduction Using Vector Diagrams to Generate Shaped Inputs," *Journal of Mechanical Design*, Vol. 116, 1994, pp. 654–659.

[19] W. Singhose, S. Drezinski, and N. Singer, "Extra-Insensitive Input Shapers for Controlling Flexible Spacecraft," *Journal of Guidance, Control and Dynamics*, Vol. 19, No. 2, 1996, pp. 385–391.

[20] W. E. Singhose, A. K. Banerjee, and W. P. Seering, "Slewing Flexible Spacecraft with Deflection-Limiting Input Shaping," *Journal of Guidance, Control, and Dynamics*, Vol. 20, No. 2, 1997, pp. 291–298.

[21] T. Watanabe, T. Makida, H. A. Fujii, H. Kojima, and W. Singhose, "An Application of Input Shaping For Electrodynamic Tether System," *AIAA/AAS Astrodynamics Specialist Conference and Exhibit*, Providence, Rhode Island, August 16–19 2004. Paper 2004-5313.

[22] P. Williams, "Dynamic multibody modeling for tethered space elevators," *Acta Astronautica*, Vol. 65, 2009, pp. 399–422.

[23] M. Kim and C. D. Hall, "Control of a rotating variable-length tethered system," *Advances in the Astronautical Sciences*, Vol. 114, 2003, pp. 1713–1732.

[24] F. R. Driscoll, R. G. Lueck, and M. Nahon, "Development and validation of a lumped-mass dynamics model of a deep-sea ROV system," *Applied Ocean Research*, Vol. 22, 2007, pp. 169 – 182.

[25] B. Buckham and M. Nahon, "Dynamics simulation of low tension tethers," *OCEANS'99 MTS/IEEE. Riding the Crest into the 21st Century.*, Vol. 2, 1999, pp. 757 – 766.

[26] T. P. Dreyer and D. M. Murray, "On the modeling of two-dimensional segmented representations of cable shape," *Ocean Engineering*, Vol. 11, No. 6, 1984, pp. 609 – 625.

[27] O. Ore, *Niels Henrik Abel: Mathematician Extraordinary*. U of Minnesota Press, 1st ed., 1957.

[28] R. G. Ayoub, "Paolo Ruffini's contributions to the quintic," *Archive for History of Exact Sciences*, Vol. 23, No. 3, 1980, pp. 253–277.

[29] A. Tustin, "A method of analyzing the behavior of linear system in terms of time series," *JIEE, London*, Vol. 94, No. IIA, 1947, pp. 130–142.